Segmentation of the Endocardial Wall of the Left Atrium using Local Region-Based Active Contours and Statistical Shape Learning

Yi Gao,[a] Behnood Gholami,[b] Robert S. MacLeod,[c] Joshua Blauer,[c] Wassim M. Haddad,[b] and Allen R. Tannenbaum[a,d]

[a] Department of Biomedical Engineering, Georgia Institute of Technology, Atlanta, GA, 30332
[b] School of Aerospace Engineering, Georgia Institute of Technology, Atlanta, GA, 30332
[c] Scientific Computing and Imaging Institute, University of Utah, Salt Lake City, UT, 84112
[d] School of Electrical & Computer Engineering, Georgia Institute of Technology, Atlanta, GA, 30332, and Technion, IIT

ABSTRACT

Atrial fibrillation, a cardiac arrhythmia characterized by unsynchronized electrical activity in the atrial chambers of the heart, is a rapidly growing problem in modern societies. One treatment, referred to as *catheter ablation*, targets specific parts of the left atrium for radio frequency ablation using an intracardiac catheter. Magnetic resonance imaging has been used for both pre- and and post-ablation assessment of the atrial wall. Magnetic resonance imaging can aid in selecting the right candidate for the ablation procedure and assessing post-ablation scar formations. Image processing techniques can be used for automatic segmentation of the atrial wall, which facilitates an accurate statistical assessment of the region. As a first step towards the general solution to the computer-assisted segmentation of the left atrial wall, in this paper we use shape learning and shape-based image segmentation to identify the endocardial wall of the left atrium in the delayed-enhancement magnetic resonance images.

Keywords: Atrial fibrillation, ablation therapy, active contours, shape-based segmentation

1. INTRODUCTION

Atrial fibrillation, a cardiac arrhythmia characterized by unsynchronized electrical activity in the atrial chambers of the heart, is a rapidly growing problem in modern societies. Electrical cardioversion and antiarrhythmic drugs are used to manage this condition, but suffer from low success rates and involve major side effects.[1–4] In an alternative treatment, known as *catheter ablation*, specific parts of the left atrium are targeted for radio frequency ablation using an intracardiac catheter.[5] Application of radio frequency energy to the cardiac tissue causes thermal injury (lesions), which in turn results into scar tissue. Successful ablation can eliminate, or isolate, the problematic sources of electrical activity and effectively cure atrial fibrillation.

Magnetic resonance imaging (MRI) has been used for both pre- and and post-ablation assessment of the atrial wall.[6] MRI can aid in selecting the right candidate for the ablation procedure and assessing post-ablation scar formations. Image processing techniques can be used for automatic segmentation of the atrial wall, which facilitates an accurate statistical assessment of the region. As a first step towards the general solution to the computer-assisted segmentation of the left atrial wall, in this paper we propose a shape-based image segmentation framework to segment the endocardial wall of the left atrium.

Further author information: (Send correspondence to B.G.)
Y.G.: E-mail: yi.gao@gatech.edu, Telephone: (404) 385-5062
B.G.: E-mail: behnood@gatech.edu, Telephone: (404) 894-3474
R.S.M.: E-mail: macleod@cvrti.utah.edu, Telephone: (801) 585-7596
J.B.: E-mail: blauer@sci.utah.edu, Telephone: (801) 585-0611
W.M.H: E-mail: wm.haddad@aerospace.gatech.edu, Telephone: (404) 894-1078
A.R.T.: E-mail: tannenba@ece.gatech.edu, Telephone: (404) 894-7582

Medical Imaging 2010: Image Processing, edited by Benoit M. Dawant, David R. Haynor,
Proc. of SPIE Vol. 7623, 76234Z · © 2010 SPIE · CCC code: 1605-7422/10/$18 · doi: 10.1117/12.844321

A powerful approach in medical image segmentation is active contour modeling wherein the boundaries of an object of interest are captured by minimizing an energy functional.[7,8] The segmentation of the endocardial wall of the left atrium in delayed-enhancement magnetic resonance images (DE-MRI) using active contours is a challenging problem mainly due to the absence of clear boundaries. This usually leads either to contour "leaks," where the contour expands beyond the desired boundary, or partial segmentation, where the contour only captures the desired area partially. A shape-based segmentation approach can overcome this problem by using prior shape knowledge in the segmentation process. In this paper, we use shape learning and shape-based image segmentation to identify the endocardial wall of the left atrium in the delayed-enhancement magnetic resonance images.

The outline of the paper is as follows. In Section 2, we present the shape learning and shape-based image segmentation framework. Next, in Section 3, this framework is applied to the problem of segmentation of the endocardial wall of the left atrium. Finally, in Section 4 we state conclusions and directions for future research.

2. SHAPE LEARNING AND SHAPE-BASED IMAGE SEGMENTATION

In this section, we propose a shape-based image segmentation framework using the work of Refs. 9 and 10 to segment the endocardial wall of the left atrium. Our proposed approach involves two steps; namely, shape learning and image segmentation. To elucidate this, let the training set be composed of N binary images $B_i : \Omega \to \{0,1\}$, $i = 1,\ldots,N$, where $\Omega \subset \mathbb{R}^3$ is the image domain. The binary image B_i corresponds to the segmentation of the endocardial wall of the left atrium for the image $I_i : \Omega \to \mathbb{R}$, $i = 1,\ldots,N$, performed by a human expert. For $i = 1,\ldots,N$, $B_i(x) = 1$ if x falls inside the left atrial chamber and $B_i(x) = 0$ otherwise.

The first step in shape learning involves image registration. The goal in image registration is to align two given images, namely, the *fixed image* and the *moving image*, by finding a homeomorphism that maps the points in the moving image to the corresponding points in the fixed image. One of the most widely used techniques in image segmentation is the energy-based technique, where an energy functional describing the similarity between the two images is maximized (or, equivalently, an energy functional describing the discrepancy between the the two images is minimized) subject to a regularization constraint.[11] Here, we consider a special class of energy-based registration techniques, namely, the *mean-square-error affine registration scheme*, which is implemented in the insight segmentation and registration toolkit (ITK).[12] While we consider binary images in this paper, the mean-square-error affine registration scheme is applicable to any gray-scale image and is not limited to binary images.

Mean-Square-Error Affine Registration. Given the fixed image $B_{\mathrm{f}} : \Omega \to \{0,1\}$ and the moving image $B_{\mathrm{m}} : \Omega \to \{0,1\}$, where $\Omega \subset \mathbb{R}^3$, the goal of the mean-square-error affine registration scheme is to find an affine transformation $\mathcal{M} : \Omega \to \Omega$ such that the cost functional

$$J(A,T) \triangleq \int_{\Omega} \left(B_{\mathrm{m}}(\mathcal{M}(x)) - B_{\mathrm{f}}(x)\right)^2 \mathrm{d}x \tag{1}$$

is minimized, where $\mathcal{M}(x) \triangleq Ax + T$ with $A \in \mathcal{R}$ and $T \in \mathbb{R}^3$ denoting a rotation matrix and translation vector, respectively, and $\mathcal{R} \subset \mathbb{R}^{3\times 3}$ denoting the set of rotation matrices.

The mean-square-error affine registration scheme is an optimization problem which can be used to register the training images. Specifically, given the training set $\{B_1,\ldots,B_N\}$ with $B_i : \Omega \to \{0,1\}$, $i = 1,\ldots,N$, the mean-square-error affine registration scheme is used to register all binary images in the training set to an arbitrary binary image from the training set denoted by B_k, $k \in \{1,\ldots,N\}$. Hence, for $k \in \{1,\ldots,N\}$, B_k is regarded as the fixed image and B_i, $i = 1,\ldots,N$, $i \neq k$, is regarded as the moving image. This results in $N-1$ mean-square-error registration problems given by

$$\min_{(A_i,T_i)\in\mathcal{R}\times\mathbb{R}^3} J_i^k(A_i,T_i), \quad A_i \in \mathbb{R}^{3\times 3},\ T_i \in \mathbb{R}^3,\ i = 1,\ldots,N,\ i \neq k, \tag{2}$$

where

$$J_i^k(A_i,T_i) \triangleq \int_{\Omega} \left(B_i(A_i x + T_i) - B_k(x)\right)^2 \mathrm{d}x.$$

We denote the registered binary moving images by $\hat{B}_i(x) \triangleq B_i(A_i^* x + T_i^*)$, $i = 1, \ldots, N$, $i \neq k$, and the binary fixed image by $\hat{B}_k(x) \triangleq B_k(x)$, $x \in \Omega$, where A_i^* and T_i^*, $i = 1, \ldots, N$, $i \neq k$, denote the optimal solutions to the optimization problem given by (2).

Next, we use principal component analysis (PCA)[13] to learn the registered shapes and create a statistical model for the shape. We need the following definition before stating the shape learning algorithm.

DEFINITION 2.1. *Given a closed surface $\mathcal{C}$ (which could correspond to the boundary of a region of interest), the* signed distance function $\phi : \Omega \to \mathbb{R}$ *is the mapping defined by*

$$\phi(x) \triangleq \begin{cases} \text{dist}(x, \mathcal{C}), & x \notin \mathcal{V}, \\ -\text{dist}(x, \mathcal{C}), & x \in \mathcal{V}, \end{cases} \tag{3}$$

where $\mathcal{V}$ is the volume enclosed by the closed surface $\mathcal{C}$ and $\text{dist}(\cdot, \cdot)$ *is the distance operator defined by* $\text{dist}(x, \mathcal{C}) \triangleq \inf_{y \in \mathcal{C}} \|x - y\|$, $x \in \Omega$.

In Ref. 9, the authors use the signed distance function to implicitly represent the training shapes, where the boundary of the training shape $\hat{B}_i(x)$, $x \in \Omega$, $i = 1, \ldots, N$, is given by the zero-level set of the signed distance function. In this paper, we use a specific discrete approximation to the signed distance function, referred to as *sparse field level sets* (SFLS),[14] for the numerical implementation. Let $\Omega_{\text{s}} \subset \mathbb{R}^3$ denote the sampled image domain, where we use the $N_1 \times N_2 \times N_3$ image grid to sample Ω with N_j, $j = 1, 2, 3$, denoting the number of grid points in the j-th coordinate. In this case, the SFLS function $\Psi_i : \Omega_{\text{s}} \to \mathbb{R}$, $i = 1, \ldots, N$, associated with the binary image B_i satisfies

$$\Psi_i(x) > 0, \quad \text{if } x \notin \mathcal{A}_i, \tag{4}$$

$$\Psi_i(x) = 0, \quad \text{if } x \in \partial\mathcal{A}_i, \tag{5}$$

$$\Psi_i(x) < 0, \quad \text{if } x \in \mathcal{A}_i,\ x \notin \partial\mathcal{A}_i, \tag{6}$$

where $\mathcal{A}_i \triangleq \{x \in \Omega_{\text{s}} : B_i(x) = 1\}$ and $\partial\mathcal{A}_i$ denotes the boundary of $\mathcal{A}_i$. Sparse field level sets, which can be regarded as a variation of narrow-band methods,[15] are an approximation to signed distance functions where the SFLS function assumes the same value as the signed distance function in the vicinity of the zero-level set. For points $x \notin \mathcal{A}_i$ (resp., $x \in \mathcal{A}_i$, $x \notin \partial\mathcal{A}_i$) which are sufficiently far from the zero-level set $\partial\mathcal{A}_i$, $\Psi_i(x) = 3$ (resp., $\Psi_i(x) = -3$).

Although the SFLS method was originally proposed in Ref. 14 to reduce the computational complexity of solving the partial differential equation governing the evolution of the level set, we use SFLS for shape representation in the shape learning stage to control the variability of the level sets for points far from the zero-level set. Using SFLS to implicity represent the shape, as opposed to the more traditional signed distance function, is particularly important in PCA shape learning. Among all possible subspaces of a fixed dimension, PCA identifies the subspace in which the projection of the data has the maximum variance. Since we are only interested in the shape represented by the zero-level set, it is desired that PCA only reflect the variations in the zero-level set and not be influenced by the variations of the level set function at points far from the zero-level set. The SFLS function reduces this variability in the value of the level set functions $\Psi_1, \ldots, \Psi_N$ by assigning a constant value to points far from the level set. Note that SFLS representation is also used in the implementation of the localized region-based active contour described later in this section to reduce the computational complexity of the level set evolution.

We use the shape-learning framework proposed in Ref. 9 using PCA. First, the mean shape given by $\bar{\Phi} \triangleq \frac{1}{N}\sum_i^N \Psi_i$ is computed. Then, the mean-offset function is defined by $\tilde{\Psi}_i \triangleq \Psi_i - \bar{\Phi}$, $i = 1, \ldots, N$. Note that $\tilde{\Psi}_i : \Omega_{\text{s}} \to \mathbb{R}$, $i = 1, \ldots, N$, where Ω_{s} is obtained by sampling Ω using the image grid. The $N_1 \times N_2 \times N_3$ image grid can be used to label each point in Ω_{s}, and hence, $\tilde{\Psi}_i$ can be transformed into an array of the size $N_1 \times N_2 \times N_3$. Next, we construct $s_i \in \mathbb{R}^M$, $i = 1, \ldots, N$, by forming a vector from the elements of the $N_1 \times N_2 \times N_3$ array associated with $\tilde{\Psi}_i$, where $M = N_1 \times N_2 \times N_3$ is the number of voxels in the binary image B_i, $i = 1 \ldots, N$. Define $S \triangleq [s_1, \ldots, s_N] \in \mathbb{R}^{M \times N}$ and $W \triangleq \frac{1}{N} S^{\text{T}} S$. Finally, we use the Schur decomposition to obtain

$$W = Q^{\text{T}} \Lambda Q, \tag{7}$$

where $Q \triangleq [q_1, \ldots, q_N]$, $q_i \in \mathbb{R}^N$, and $\Lambda \triangleq \mathrm{diag}[\lambda_1, \ldots, \lambda_N]$. The normalized eigenshapes Φ_i, $i = 1, \ldots, N$, are given by $\Phi_i = \frac{1}{\|Sq_i\|} Sq_i \in \mathbb{R}^M$, where we assume that their corresponding eigenvalues λ_i, $i = 1, \ldots, N$, are in decreasing order, $Sq_i \neq 0$, $i = 1, \ldots, N$, and $\|\cdot\|$ denotes the Euclidean norm on $\mathbb{R}^M$.

In the framework proposed in Ref. 9, given a new image $I : \Omega \to \mathbb{R}$, it is assumed that the segmenting surface represented by a level-set function can be written as a weighted sum of the eigenshapes. Due to the complexity of the optimization problem and the presence of local minima, the initial guess in the optimization problem affects the optimal solution provided by the numerical algorithm. In this paper, we introduce an intermediate step in which we use localized region-based active contours proposed by Ref. 10 to provide a better initialization to the optimization problem.

The localized region-based active contours provide a framework for segmenting heterogenous objects, where both global region-based and local edge-based methods fail.[10] The contour is implicitly represented by the signed distance function $\phi : \Omega \to \mathbb{R}$, where in our implementation we use the SFLS to represent ϕ due to its computational efficiency. Although we consider the Chan-Vese energy functional[16] within the localized region-based active contour framework, other energy functionals can be used.[10]

For a given signed distance function ϕ define the *smoothed Heaviside function* $\mathcal{H}_\phi : \Omega \to \mathbb{R}$ by

$$\mathcal{H}_\phi(x) \triangleq \begin{cases} 1, & \phi(x) < \epsilon, \\ 0, & \phi(x) > \epsilon, \\ \frac{1}{2}\left[1 + \frac{\phi}{\epsilon} + \frac{1}{\pi}\sin\left(\frac{\pi\phi(x)}{\epsilon}\right)\right], & \text{otherwise.} \end{cases} \tag{8}$$

In this case, the derivative $\delta_\phi : \Omega \to \mathbb{R}$ of the smoothed Heaviside function with respect to $x \in \Omega$ is given by

$$\delta_\phi(x) \triangleq \begin{cases} 1, & \phi(x) = 0, \\ 0, & |\phi(x)| < \epsilon, \\ \frac{1}{2\epsilon}\left[1 + \cos\left(\frac{\pi\phi(x)}{\epsilon}\right)\right], & \text{otherwise.} \end{cases} \tag{9}$$

Moreover, for a given $r > 0$, define

$$\mathcal{B}_r(x, y) \triangleq \begin{cases} 1, & \|x - y\| < r, \\ 0, & \text{otherwise.} \end{cases} \tag{10}$$

The contour $\mathcal{C}$ segmenting the region of interest for a given image $I : \Omega \to \mathbb{R}$ is given by

$$\mathcal{C} = \{x \in \Omega : \phi^*(x) = 0\}, \tag{11}$$

where $\phi^* : \Omega \to \mathbb{R}$ is the solution of the minimization problem

$$\min_{\phi \in \mathbb{F}} E_{\mathrm{lrac}}(\phi), \tag{12}$$

where $F \triangleq \{\phi : \Omega \to \mathbb{R} : \phi \text{ is a signed distance function}\}$,

$$E_{\mathrm{lrac}} \triangleq \int_\Omega \delta_\phi(x) \int_\Omega \mathcal{B}_r(x, y) F(I(y), \phi(y)) \mathrm{d}y \mathrm{d}x + \alpha \int_\Omega \delta_\phi(x) \|\nabla\phi(x)\| \mathrm{d}x, \quad \alpha > 0, \tag{13}$$

$$F(y) \triangleq \mathcal{H}_\phi(y)(I(y) - u_x)^2 + (1 - \mathcal{H}_\phi(y))(I(y) - v_x)^2, \tag{14}$$

$$u_x \triangleq \frac{\int_\Omega \mathcal{B}_r(x, y)\mathcal{H}_\phi(y) I(y) \mathrm{d}y}{\int_\Omega \mathcal{B}_r(x, y)\mathcal{H}_\phi(y) \mathrm{d}y}, \tag{15}$$

$$v_x \triangleq \frac{\int_\Omega \mathcal{B}_r(x, y)(1 - \mathcal{H}_\phi(y)) I(y) \mathrm{d}y}{\int_\Omega \mathcal{B}_r(x, y)(1 - \mathcal{H}_\phi(y) \mathrm{d}y}, \tag{16}$$

where $\|\cdot\|$ denotes the Euclidean norm on $\mathbb{R}^3$, ∇ denotes the gradient operator, and α is a regularization parameter. Here, we use the mean shape $\bar{\Phi}$ as the initialization for the localized region-based active contour.

Next, the result of the segmentation process is considered as an initial condition for the shape-based segmentation given by Ref. 9. Specifically, define a new level set function $\Phi_{w,\mathcal{T}_p} : \Omega \to \mathbb{R}$ by

$$\Phi_{w,\mathcal{T}_p}(x) = \bar{\Psi}\left(\mathcal{T}_p(x)\right) + \sum_{i=1}^{e} \sqrt{\lambda_i} w_i \Phi_i\left(\mathcal{T}_p(x)\right), \tag{17}$$

where $w = [w_1 \ \ldots, \ w_e]^{\mathrm{T}}$, $w_i \in \mathbb{R}$, $i = 1, \ldots, e$, $e \in \mathbb{Z}_+$, $e < N$, is the number of selected eigenshapes, and $\mathcal{T}_p : \Omega \to \Omega$ is a similarity transformation with parameter vector $p \in \mathbb{R}^7$ which includes translation, rotation, and magnification. Here we use the *binary mean model*[17] for the shape-based segmentation. Finally, note that the segmented region is given by the zero-level set of the function $\Phi^*_{w,\mathcal{T}_p}$, where $\Phi^*_{w,\mathcal{T}_p}$ is the optimal solution of the optimization problem given by

$$\min_{(w,p)\in\mathbb{R}^k\times\mathbb{R}^7} E_{\mathrm{binary}}(\Phi_{w,\mathcal{T}_p}), \tag{18}$$

where

$$E_{\mathrm{binary}}(\Phi_{w,\mathcal{T}_p}) \triangleq -\frac{1}{2}\left(\frac{S_{\mathrm{u}}}{A_{\mathrm{u}}} - \frac{S_{\mathrm{v}}}{A_{\mathrm{v}}}\right)^2, \tag{19}$$

$$A_{\mathrm{u}} \triangleq \int_\Omega \hat{\mathcal{H}}_{\Phi_{w,\mathcal{T}_p}}(y)\mathrm{d}y, \tag{20}$$

$$A_{\mathrm{v}} \triangleq \int_\Omega (1 - \hat{\mathcal{H}}_{\Phi_{w,\mathcal{T}_p}}(y))\mathrm{d}y, \tag{21}$$

$$S_{\mathrm{u}} \triangleq \int_\Omega I(y)\hat{\mathcal{H}}_{\Phi_{w,\mathcal{T}_p}}(y)\mathrm{d}y, \tag{22}$$

$$S_{\mathrm{v}} \triangleq \int_\Omega I(y)(1 - \hat{\mathcal{H}}_{\Phi_{w,\mathcal{T}_p}}(y))\mathrm{d}y, \tag{23}$$

$$\hat{\mathcal{H}}_{\Phi_{w,\mathcal{T}_p}}(y) \triangleq \begin{cases} 1, & \Phi_{w,\mathcal{T}_p}(y) \le 0, \\ 0, & \Phi_{w,\mathcal{T}_p}(y) > 0. \end{cases} \tag{24}$$

3. APPLICATION TO ENDOCARDIAL WALL SEGMENTATION

In this section, we apply the framework of Section 2 to the problem of segmentation of the endocardial wall of the left atrium. Our data set includes 20 DE-MRI, namely $\{I_1, \ldots, I_{20}\}$, and their associated hand segmentations of the endocardial wall of the left atrium $B_1, \ldots, B_{20}$. These images are obtained from patients having undergone catheter ablation three months prior to the scan time. In our study, we use a hold-out method for cross-validation.[18] More specifically, the training set consists of the binary human-expert segmentations $B_6, \ldots, B_{20}$ and the test set consists of the DE-MR images $I_1, \ldots, I_5$. The segmentation results provided by the algorithm can be compared to the human-expert segmentations $B_1, \ldots, B_5$.

In the first step of the algorithm, the binary images in the training set $\{B_6, \ldots, B_{20}\}$ are registered to an arbitrary binary image, e.g., B_6. Next, the SFLS representation described in the previous section is used to implicitly represent the training shapes. After subtracting the mean shape from all the training shapes, PCA learning is used to find the first 8 eigenshapes and their associated eigenvalues. This concludes the training phase of the algorithm.

Next, the trained algorithm is used for the segmentation of the endocardial wall of the left atrium by applying it to the test set $\{I_1, \ldots, I_5\}$. We assume that the human user can provide the algorithm with an approximate estimate of the centroid coordinates of the left atrium by a mouse click. Next, a translation transformation is applied to the mean shape so that its centroid coincides with the approximate centroid coordinates of the left atrium provided by the human user. The translated mean shape is used as an initialization for the localized region-based active contour algorithm. In the last step of the algorithm, the segmentation provided by the localized region-based active contour algorithm is used as an initialization for the shape-based segmentation algorithm described in the previous section. Table 1 outlines the proposed algorithm. The 3-dimensional and 2-dimensional view of the segmented endocardial wall of the left atrium for Patient 1 are given in Figure 1 and Figure 2, respectively.

Table 1. Endocardial Wall Segmentation Algorithm

Step 1. Shape Learning.
- **a.** Register binary images $B_7, \ldots, B_{20}$ to B_6 using the mean-square-error affine registration scheme. Denote the registered training images by $\hat{B}_6, \ldots, \hat{B}_{20}$.
- **b.** Use SFLS to represent $\hat{B}_6, \ldots, \hat{B}_{20}$. Denote by $\Psi_6, \ldots, \Psi_{20}$.
- **c.** Compute the mean shape $\bar{\Phi}$. Compute the mean-offset functions $\tilde{\Psi}_6, \ldots, \tilde{\Psi}_{20}$.
- **d.** Construct $s_6, \ldots, s_{20}$ by forming a vector from the elements of $\tilde{\Psi}_6, \ldots, \tilde{\Psi}_{20}$.
- **e.** Compute $S = [s_1, \ldots, s_N]$ and $W = \frac{1}{N} S^{\mathrm{T}} S$.
- **f.** Use the Schur decomposition to obtain $W = Q^{\mathrm{T}} \Lambda Q$, where $Q = [q_1, \ldots, q_N]$ and $\Lambda = \mathrm{diag}[\lambda_1, \ldots, \lambda_N]$.
- **g.** Compute the normalized eigenshapes $\Phi_i = \frac{1}{\|Sq_i\|} Sq_i$.
- **h.** Select the first e eigenshapes corresponding to the largest eigenvalues. Denote by $\Phi_1, \ldots, \Phi_e$.

Step 2. Image Segmentation.
- **a.** **for** $j = 1 : 5$
- **b.** Initialize the localized region-based active contour evolution for DE-MR image I_j using the mean-shape $\bar{\Phi}$ found in **Step 1c**.
- **c.** Evolve the segmenting surface $\mathcal{C}$ until some convergence criterion is met.
- **d.** Solve the optimization problem (18). Use the result of **Step 2c** as an initial guess for the optimization problem.
- **e.** **end for**

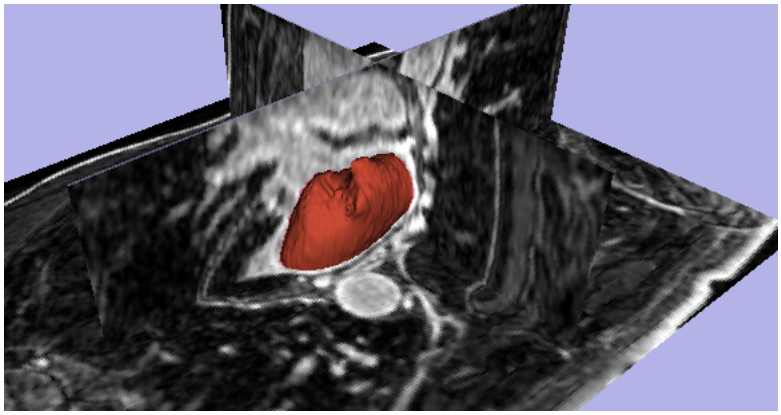

Figure 1. 3-dimensional view of the segmentation of the endocardial wall of the left atrium.

4. CONCLUSION

In this paper, we proposed a shape-based image segmentation framework to segment the endocardial wall of the left atrium. The segmentation of the endocardial wall of the left atrium in delayed-enhancement magnetic resonance images using active contours is a challenging problem mainly due to the absence of clear boundaries. It was shown that a shape-based segmentation approach can overcome this problem by using prior shape knowledge in the segmentation process. Our proposed approach involved shape learning and image segmentation.

Future work will include extending this framework to segment the epicardial wall, and ultimately, the automatic segmentation of the atrial wall. In addition, we will use computer-aided statistical assessment of the enhanced regions in the DE-MRI which can greatly benefit the study of ablation therapy for atrial fibrillation patients.

Acknowledgements. This research was supported in part by a grant from NIH (NAC P41 RR-13218) through Brigham and Women's Hospital and by the US Army Medical Research and Material Command under

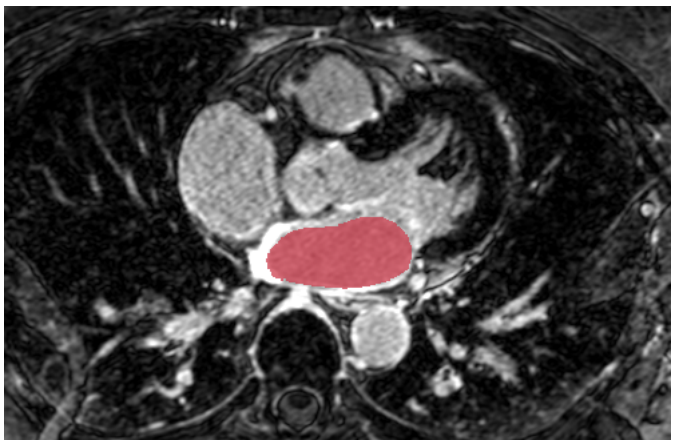

Figure 2. 2-dimensional view of the segmentation of the endocardial wall of the left atrium.

grant 08108002. This work is part of the National Alliance for Medical Image Computing (NAMIC), funded by the National Institutes of Health through the NIH Roadmap for Medical Research, Grant U54 EB005149. Information on the National Centers for Biomedical Computing can be obtained at `http://nihroadmap.nih.gov/bioinformatics`.

REFERENCES

[1] Falk, R. H., "Atrial fibrillation," *N. Engl. J. Med.* **344**(14), 1067–1078 (2001).

[2] Gelder, I. C. V., Crijns, H. J., Tieleman, R. G., Brugemann, J., Kam, P. J. D., Gosselink, A. T., Verheugt, F. W., and Lie., K. I., "Chronic atrial fibrillation: Success of serial cardioversion therapy and safety of oral anticoagulation," *Arch. Intern. Med.* **156**(22), 2585–2592 (1996).

[3] Brodsky, M. A., Allen, B. J., Walker, C. J., Casey, T. P., Luckett, C. R., and Henry, W. L., "Amiodarone for maintenance of sinus rhythm after conversion of atrial fibrillation in the setting of a dilated left atrium," *Am. J. Cardiol.* **60**, 572–575 (1987).

[4] Crijns, H. J., Gelder, I. C. V., der Woude, H. J. V., Grandjean, J. G., Tieleman, R. G., Brugemann, J., Kam, P. J. D., and Ebels, T., "Efficacy of serial electrical cardioversion therapy in patients with chronic atrial fibrillation after valve replacement and implications for surgery to cure atrial fibrillation," *Am. J. Cardiol.* **78**, 1140–1144 (1996).

[5] Jais, P., Weerasooriya, R., Shah, D. C., Hocini, M., Macle, L., Choi, K.-J., Scavee, C., Haissaguerre, M., and Clementy, J., "Ablation therapy for atrial fibrillation: Past, present, and future," *Cardiovas. Res.* **54**, 337–346 (2002).

[6] McGann, C. J., Kholmovski, E. G., Oakes, R. S., Blauer, J. E., Daccarett, M., Segerson, N. M., Airey, K. J., Akoum, N., Fish, E. N., Badger, T. J., DiBella, E. V. R., Parker, D., MacLeod, R. S., and Marrouche, N. F., "New magnetic resonance imaging based method to define extent of left atrial wall injury after the ablation of atrial fibrillation," *J. Am. Coll. Cardiol.* **52**(15), 1263–1271 (2008).

[7] Blake, A. and Isard, M., [*Active Contours*], Springer-Verlag, New York, NY (1998).

[8] Caselles, V., Kimmel, R., and Sapiro, G., "Geodesic active contours," *Int. J. Comp. Vis.* **22**(1), 61–79 (1997).

[9] Tsai, A., Yezzi, A., Wells, W., Tempany, C., Tucker, D., Fan, A., Grimson, W. E., and Willsky, A., "A shape-based approach to the segmentation of medical imagery using level sets," *IEEE Trans. Med. Imag.* **22**(2), 137–154 (2003).

[10] Lankton, S. and Tannenbaum, A. R., "Localizing region-based active contours," *IEEE Trans. Imag. Proces.* **17**, 2029–2039 (2008).

[11] Toga, A. W., [*Brain Warping*], Academic Press, San Diego, CA (1999).

[12] Ibanez, L., Schroeder, W., Ng, L., and Cates, J., [*The ITK Software Guide*], second ed. (2005). http://www.itk.org/ItkSoftwareGuide.pdf.

[13] Jolliffe, I. T., [*Principal Component Analysis*], Springer (2002).

[14] Whitaker, R. T., "A level-set approach to 3D reconstruction from range data," *Int. J. Comp. Vis.* **29**(3), 203–231 (1998).

[15] Adalstein, D. and Sethian, J. A., "A fast level set method for propogating interfaces," *J. Comput. Phys.* **118**, 269–277 (1995).

[16] Chan, T. F. and Vese, L. A., "Active contours without edges," *IEEE Trans. Imag. Proces.* **10**, 266–277 (2001).

[17] Yezzi, A., Tsai, A., and Wilsky, A., "A statistical approach to snakes for bimodal and trimodal imagery," in [*Proc. Int. Conf. Comp. Vis.*], 898–903 (1999).

[18] Bishop, C. M., [*Pattern Recognition and Machine Learning*], Springer, New York, NY (2006).